Geophysical Journal International

Geophys. J. Int. (2014) **197,** 910–919
Advance Access publication 2014 February 27

doi: 10.1093/gji/ggu045

Effect of Fe-enrichment on seismic properties of perovskite and post-perovskite in the deep lower mantle

S.M. Dorfman[1] and T.S. Duffy[2]

[1]*Earth and Planetary Science Laboratory, Ecole polytechnique fédérale de Lausanne, Station* 3, *CH*-1015 *Lausanne, Switzerland.*
E-mail: susannah.dorfman@epfl.ch
[2]*Department of Geosciences, Princeton University, Princeton, NJ* 08544, *USA*

Accepted 2014 February 3. Received 2014 January 27; in original form 2013 October 22

SUMMARY

Recent experimental measurements of the equation of state of perovskites and post-perovskites in the (Mg,Fe)SiO_3 and (Mg,Fe,Al)(Fe,Al,Si)O_3 systems over a wide range of iron contents are used to constrain the effects of Fe and Al on density and bulk modulus of these phases at deep mantle pressures. The density of Fe-bearing perovskite follows a linear relationship with Fe-content at a representative mid-mantle depth of 1850 km (80 GPa): ρ_{80} (g cm^{-3}) = 5.054(1) + 1.270(3)X_{Fe}. The bulk modulus of silicate perovskite is not sensitive to Fe-content and follows the relationship, K_{80} (GPa) = 546(2) + 12(25)X_{Fe}. The velocity heterogeneity parameter, $\partial \ln V_B/\partial X_{Fe}$, determined by experimental values for the bulk sound speed is 0.10(1), in agreement with theory and the behaviour of other Fe-bearing silicates. Near the core–mantle boundary, Fe-rich post-perovskite is observed to be more compressible than the Mg-end-member, in contrast to theoretical predictions. From experimental data, the densities of perovskite and post-perovskite at 125 GPa (2700 km depth) are $\rho_{125,Pv}$ (g cm^{-3}) = 5.426(11) + 1.38(4)X_{Fe} and $\rho_{125,pPv}$ (g cm^{-3}) = 5.548(1) + 1.41(3)X_{Fe}. The density contrast across the post-perovskite transition is ∼2 per cent, irrespective of Fe-content, but the contrast in bulk sound speed increases with Fe-content. Al-rich silicates exhibit no significant differences in density or compressibility relative to Al-free silicates, but may be responsible for seismic heterogeneities due to differences in the depth and width of the post-perovskite transition. Observations of increased densities in large low shear velocity provinces and ultra-low-velocity zones may be consistent with local iron enrichment from Mg#90 to Mg# 78–88 and Mg# <50, respectively.

Key words: Composition of the mantle; Equations of state; High-pressure behaviour.

1 INTRODUCTION

Chemical heterogeneity in the deep lower mantle has been constrained by geophysical observations and dynamic simulations (Stixrude & Lithgow-Bertelloni 2012). Thermal variation alone cannot explain observations of anticorrelated bulk and shear wave speeds in the deep mantle (e.g. Masters *et al.* 2000). In addition, seismic images of large (∼1500 km) low shear velocity provinces (LLSVPs) beneath the Pacific and Africa have features such as sharp lateral gradients at their edges that are suggestive of compositional heterogeneity (McNamara & Zhong 2004, 2005). From normal mode data, Ishii & Tromp (1999) reported that regions of high density were associated with low velocities in the two plume provinces. LLSVPs could represent hot dense piles of compositionally distinct material or buoyant thermal superplumes and these models would be expected to have different degrees of chemical heterogeneity and distinct density structures.

The Earth's core–mantle boundary region (D″) also exhibits highly-variable localized structure and is therefore also likely to be chemically heterogeneous (Garnero 2000). Heterogeneities could possibly form due to accumulations of subducted crust (Dobson & Brodholt 2005; Hutko *et al.* 2006), remnant primordial material (Labrosse *et al.* 2007) or core–mantle interaction (Knittle & Jeanloz 1989, 1991). Waveform modelling has led to the identification of ultra-low velocity zones (ULVZs) just above the core–mantle boundary (Garnero & Helmberger 1995). These ULVZs tend to be distributed at the margins of LLSVPs and exhibit strong reductions (>10 per cent) in *P*- and *S*-wave velocities. ULVZs are thin and typically localized (∼5–40 km thick and ∼100 km wide) with a large increase in density (∼10 per cent) compared with surrounding material (Rost & Garnero 2006). These properties could possibly be signatures of dense melts (Williams & Garnero 1996) or iron-enriched solid mantle phases (Mao *et al.* 2006; Wicks *et al.* 2010). The role of iron is thus one of the major factors

to consider in assessing compositional heterogeneity in the lower mantle.

Determining the behaviour of iron in the lower mantle's dominant phase, $(Mg,Fe,Al)(Fe,Al,Si)O_3$ perovskite, is complex because Fe can occupy different structural sites with different valence and spin states, which may differently affect seismic properties (e.g. Caracas 2010a). In addition, Fe has been observed to affect the depth and breadth of the transition of mantle perovskite to the post-perovskite structure, with important implications for the phase assemblage near the core–mantle boundary (Murakami *et al.* 2004; Oganov & Ono 2004; Mao *et al.* 2004, 2005). Partitioning of Fe between multiple Fe-bearing mantle phases is also important to phase transformations and physical properties (Grocholski *et al.* 2012). However, modelling of the effect of Fe on mantle phases has generally been simplified in studies to date. For example, Trampert *et al.* (2001) and Mattern *et al.* (2005) constructed lower-mantle mineral models in which Fe affects the thermoelastic properties of silicate perovskite only through its effect on the molar volume at ambient pressure, which is far from thermodynamic stability and so can exhibit considerable scatter among experimental determinations (Kiefer *et al.* 2002; Tange *et al.* 2009). Recent experimental data on Fe-bearing mantle silicates at mantle pressures has allowed improved modelling of the complexity of Fe-dependence of elastic properties (Nakagawa *et al.* 2012).

Compression studies using X-ray diffraction as a probe provide many of the existing experimental constraints on elasticity of lower-mantle materials. In this work, we synthesize experimental equation of state measurements on perovskites and post-perovskites with a wide range of compositions and compare with theoretical calculations to assess the current understanding of the equation of state of deep mantle silicates. We discuss the dependence of density and seismic wave velocity on Fe- and Al-content in perovskite and post-perovskite. We investigate the implications of these chemical effects for deep lower-mantle heterogeneities.

2 ANALYSIS

A number of recent studies have carried out 300-K equation of state measurements on perovskite and post-perovskite phases synthesized in the $(Mg,Fe)SiO_3$ and $(Mg,Fe,Al)(Fe,Al,Si)O_3$ systems (Walter *et al.* 2004; Guignot *et al.* 2007; Lundin *et al.* 2008; Nishio-Hamane *et al.* 2008; Shim *et al.* 2008; Nishio-Hamane & Yagi 2009; Catalli *et al.* 2010b, 2011; Shieh *et al.* 2011; Boffa Ballaran *et al.* 2012; Zhang *et al.* 2012; Dorfman *et al.* 2012b, 2013). These studies used synchrotron X-ray diffraction in the laser-heated diamond anvil cell (Duffy 2005) to synthesize the high-pressure phases and to measure their unit cell volumes as a function of pressure. The compositions studied involve a variety of cation substitutions and possible cation site occupancies. In particular, a number of these recent studies have focused on Fe- and Al-rich samples, thereby allowing compositional trends to be better constrained. The Fe fraction ($X_{Fe} = 2\,Fe/[Mg + Fe + Al + Si]$) over the combined A and B sites of the ABO_3 stoichiometries ranged from 0 to 0.75. In addition, compositions with Al_2O_3 contents as high as 25 mole per cent have been studied (Walter *et al.* 2004; Shieh *et al.* 2011; Boffa Ballaran *et al.* 2012; Dorfman *et al.* 2012b).

In most of these studies, the valence state of Fe in synthesized perovskites and post-perovskites was not measured directly. *In-situ* Mössbauer spectroscopy and *ex-situ* electron energy loss spectroscopy measurements of $Fe^{3+}/\Sigma Fe$ ratios in perovskites and post-perovskites synthesized from Al-free, Fe^{2+}-bearing starting materials range from 0.08 to 0.5, with a median value of 0.16 (McCammon 1997; Frost & Langenhorst 2002; Li *et al.* 2004; Jackson *et al.* 2005; Sinmyo *et al.* 2008; Mao *et al.* 2011b; Sinmyo *et al.* 2011). Al-content is well-known to promote higher $Fe^{3+}/\Sigma Fe$ in perovskite, typically 0.5–0.8 (McCammon 1997; Frost & Langenhorst 2002; Sinmyo *et al.* 2011). However, crystallographic differences observed between perovskites synthesized from $(Mg,Fe^{2+},Al)(Al,Si)O_3$ and $(Mg,Fe^{3+})(Al,Si)O_3$-bearing compositions may indicate that ferrous iron can be preserved in aluminous perovskites (Dorfman *et al.* 2012b). The $Fe^{3+}/\Sigma Fe$ ratio in post-perovskite has been observed to be close to that of the starting material (Sinmyo *et al.* 2011). When discussing ferrous or ferric iron content in this work, we refer to measured compositions of starting materials.

In comparison of experimental studies at deep mantle conditions, a concern involves the consistency of pressure determination and hydrostatic stress conditions among different works (Fei *et al.* 2007; Dorfman *et al.* 2012a). The studies under consideration here all used an internal pressure standard for which the equation of state was determined with reference to shock compression or other data. Most of the studies (Lundin *et al.* 2008; Nishio-Hamane *et al.* 2008; Nishio-Hamane & Yagi 2009; Catalli *et al.* 2010b, 2011; Shieh *et al.* 2011; Dorfman *et al.* 2013, 2012b) used Au as an internal pressure standard; for the scales chosen in these studies (Tsuchiya 2003; Dewaele *et al.* 2004; Fei *et al.* 2007), errors due to pressure calibration differences are expected to be minimal (<1.5 GPa). In other studies, use of KCl, NaCl, MgO or Pt may lead to systematic differences in pressure determination. At Mbar pressures, the Pt and NaCl scales were observed to give pressures up to 5–10 GPa lower than Au (Dorfman *et al.* 2012a). As a result, studies using these other calibrants measured perovskite and post-perovskite volumes, V, systematically lower by up to 1.5 per cent. Differences in bulk modulus, K, due to pressure calibration are negligible with respect to other uncertainties. Systematic differences may also be observed in calibrant and sample volumes due to non-hydrostatic stress in the diamond anvil cell. Most of the studies considered here used soft media such as Ne and laser annealing, which minimize non-hydrostatic stress (Dorfman *et al.* 2012a).

Pressure–volume data were fit to the Birch–Murnaghan equation (Birch 1947) to allow interpolation of volumes to common reference pressures. Densities, ρ, were calculated from volumes using the known chemical compositions of the samples. The isothermal bulk modulus, $K = -V(\partial P/\partial V)_T$, was obtained at reference pressures from differentiation of the Birch–Murnaghan equation with respect to volume (Jackson 1998). The bulk sound velocity was calculated from K and ρ: $V_B = \sqrt{K/\rho}$. The difference between the adiabatic and isothermal bulk modulus is small relative to experimental uncertainties and was neglected. The corresponding expressions for the compressional (V_P) and shear (V_S) wave velocities are $V_P = \sqrt{(K + 4G/3)/\rho}$ and $V_S = \sqrt{G/\rho}$, where G is the shear modulus.

2.1 Perovskite

The pressure range of experimental volume compression data for $(Mg,Fe)SiO_3$ compositions was 0–100 GPa (Lundin *et al.* 2008; Dorfman *et al.* 2013) and for $(Mg,Fe)_3Al_2Si_3O_{12}$ was 0–150 GPa (Walter *et al.* 2004; Dorfman *et al.* 2012b) compositions (Fig. 1). $(Mg,Fe)_3Al_2Si_3O_{12}$ is the pyrope–almandine garnet system which transforms to single-phase perovskites $((Mg,Fe)_{0.75}Al_{0.25})(Al_{0.25}Si_{0.75})O_3$ above 40–70 GPa (Irifune *et al.*

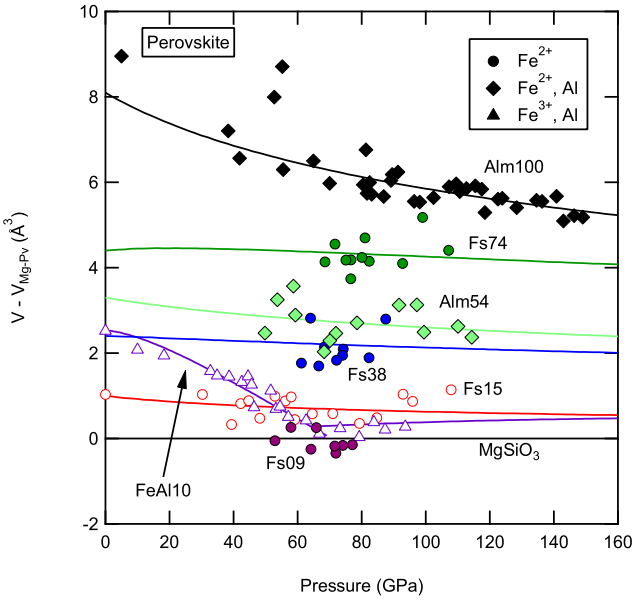

Figure 1. Volume differences between Fe- or Fe, Al-bearing perovskites and $MgSiO_3$ perovskite (Lundin *et al.* 2008). Fe-bearing perovskite with $FeSiO_3$ (Fs) from 9–74 per cent is shown in circles (Lundin *et al.* 2008; Dorfman *et al.* 2013). Perovskites synthesized from pyrope–almandine (Alm) compositions with 54 and 100 per cent Alm are displayed with diamonds (Dorfman *et al.* 2012b). Ten per cent $FeAlO_3$ composition (Catalli *et al.* 2011) is shown in triangles. Curves shown are from Birch–Murnaghan equation of state fits.

1996; Walter *et al.* 2004; Dorfman *et al.* 2012b). Relative to the Mg end-member, $(Mg,Fe)SiO_3$ perovskite unit cell volumes increase approximately linearly with Fe-content independent of pressure. Incorporation of Al increases the unit cell volume of perovskite more at low pressure (Yagi *et al.* 2004; Saikia *et al.* 2009) than at deep lower-mantle pressures (Walter *et al.* 2004; Catalli *et al.* 2011). This difference may be the result of a change of mechanism of Al-incorporation from vacancy to coupled substitution (Brodholt 2000; Andrault *et al.* 2007).

To allow direct comparison between different studies, 80 GPa was chosen as a reference pressure (corresponding to ~1850 km depth in Earth's mantle) and the equation of state was used to calculate the density and bulk modulus at this pressure for each measured composition. The density of silicate perovskite increases with Fe-content, and the majority of the experimental data are well-described by a linear relationship (Fig. 2). For $(Mg,Fe)SiO_3$ perovskites at 80 GPa, the least-squares fit to the densities is ρ_{80} (g cm^{-3}) = 5.054(1) + 1.270(3)X_{Fe}. Recent experimental data on Fe-rich compositions (Boffa Ballaran *et al.* 2012; Dorfman *et al.* 2012b, 2013) have enabled us to provide tight constraints on the density trend to much higher iron contents than previously available.

The density of Al-bearing perovskites for a given Fe-content is similar or slightly lower than Al-free perovskites. The linear fit to densities of Fe, Al-bearing compositions is within uncertainty of the above equation for Fe-bearing, Al-free compositions. The equation of state of Fe^{3+}, Al-bearing perovskite measured by Nishio-Hamane *et al.* (2008) gives density and compressibility in good agreement with studies on Fe^{2+}-bearing compositions, despite the differences in chemistry. Fe^{3+}-bearing perovskites with densities ~2 per cent lower than comparable Fe^{2+}-bearing compositions were observed by Cataldi *et al.* (2010b) and Boffa Ballaran *et al.* (2012), possibly due to Fe-content in the perovskite B-site.

Additional constraints on effects of Fe- and/or Al-incorporation on elastic properties of silicate perovskite have been provided by *ab initio* calculations (Karki *et al.* 2001; Kiefer *et al.* 2002; Wentzcovitch *et al.* 2004; Caracas & Cohen 2005; Li *et al.* 2005; Stackhouse *et al.* 2006; Tsuchiya & Tsuchiya 2006; Zhang & Oganov 2006; Bengtson *et al.* 2007; Caracas *et al.* 2010; Caracas 2010a,b; Hsu *et al.* 2010; Umemoto *et al.* 2010; Hsu *et al.* 2011a; Huang & Pan 2012; Metsue & Tsuchiya 2012; Tsuchiya & Wang 2013). Density functional theory is not limited by experimentally accessible conditions and can provide values for both bulk and shear properties but results can depend on the choice of exchange-correlation functional. For silicates, the general gradient approximation (GGA) can suffer from underbinding leading to underestimated elastic constants and overestimated volumes, while the local density approximation (LDA) tends to produce the reverse situation (Kiefer *et al.* 2002). Some density functional theory work has also included the potential effects of Fe spin transitions on elastic properties (Bengtson *et al.* 2007; Caracas *et al.* 2010; Caracas 2010a,b; Hsu *et al.* 2010, 2011a; Huang & Pan 2012; Metsue & Tsuchiya 2012; Tsuchiya & Wang 2013). The most recent of these studies employ a Hubbard correction (LSDA+U), thought to produce more accurate results for iron-bearing minerals at high pressure (Hsu *et al.* 2011b; Metsue & Tsuchiya 2012).

Ab initio calculations for $MgSiO_3$ perovskite predict densities that agree with experimental measurements to within 3 per cent (Fig. 2; Kiefer *et al.* 2002; Caracas & Cohen 2005; Umemoto *et al.* 2010; Metsue & Tsuchiya 2012). For Fe-bearing perovskite, the increase in ρ with Fe-content predicted by the LDA method is similar to experimental measurements but systematically offset to higher density, consistent with volume underestimated by LDA. However, the densities calculated for $(Mg_{0.5}Fe_{0.5})SiO_3$ and $FeSiO_3$ compositions by Caracas & Cohen (2005) with the GGA method are significantly lower than experimental measurements.

The bulk modulus obtained from the Birch–Murnaghan equation fits to experimental volume data is insensitive to Fe-content or increases weakly (Fig. 2). A linear fit of bulk modulus at 80 GPa to composition, K_{80} (GPa) = 546(2) + 12(25)X_{Fe}, exhibits a stiffening of 2±4 per cent in K from X_{Fe}=0 to 100. These experimental data are consistent with the slope predicted by theoretical calculations (Kiefer *et al.* 2002; Caracas & Cohen 2005; Umemoto *et al.* 2010; Metsue & Tsuchiya 2012). Generally, in mantle silicates and oxides at ambient conditions, Mg,Fe-substitution only weakly affects the bulk modulus (Speziale *et al.* 2005). The adiabatic bulk moduli in the olivine–fayalite, enstatite–ferrosilite, pyrope–almandine and periclase–wüstite systems show less than a 7 per cent difference between the Fe end-member and the Mg end-member. More limited data on high-pressure silicates (wadsleyite, ringwoodite) also show a weak effect of Fe-substitution on bulk modulus (Mao *et al.* 2011a). Our results suggest that perovskites behave in a similar manner to other silicates.

The possible effect of an Fe spin transition on the equation of state and compressibility of perovskite has attracted much interest (Lin *et al.* 2013). Both Fe^{2+}- and Fe^{3+}-bearing perovskite samples have been observed by X-ray emission and Mössbauer spectroscopy techniques to undergo a transition to from high spin to low spin (Badro *et al.* 2004; Jackson *et al.* 2005; Cataldi *et al.* 2010b; McCammon *et al.* 2010; Mao *et al.* 2011b) or intermediate spin (Lin *et al.* 2008; McCammon *et al.* 2008). A spin transition in perovskite has been observed to be associated with higher K for Fe-bearing perovskite (Fig. 2; Cataldi *et al.* 2010b, 2011; Mao *et al.* 2011b). However, density functional theory calculations predict that any spin transition would have a small effect on the density and bulk modulus of

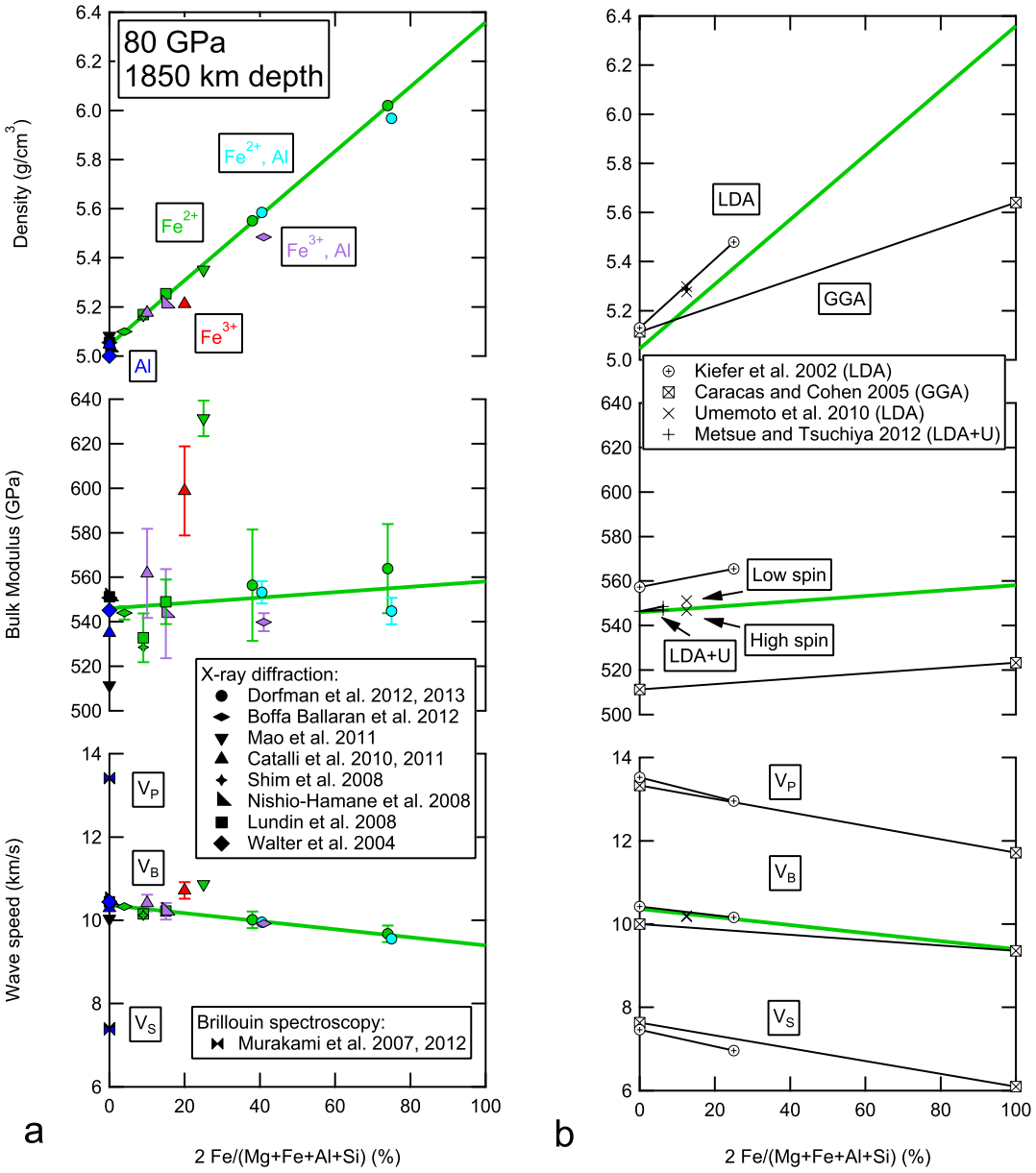

Figure 2. (a) At 80 GPa and 300 K, density, bulk modulus and seismic wave propagation speeds for perovskites with varying Fe, Al-content determined from experimental data (Walter *et al.* 2004; Murakami *et al.* 2007b; Lundin *et al.* 2008; Nishio-Hamane *et al.* 2008; Shim *et al.* 2008; Catalli *et al.* 2010b, 2011; Mao *et al.* 2011b; Boffa Ballaran *et al.* 2012; Dorfman *et al.* 2012b; Murakami *et al.* 2012; Dorfman *et al.* 2013). Bold green line fits are shown to Fe^{2+}-bearing compositions. (b) Density functional theory results at 80 GPa and 0 K for $(Mg,Fe)SiO_3$ perovskites from LDA (Kiefer *et al.* 2002; Umemoto *et al.* 2010; Metsue & Tsuchiya 2012) and GGA (Caracas & Cohen 2005).

perovskite (Fig. 2; Umemoto *et al.* 2010; Hsu *et al.* 2011a; Metsue & Tsuchiya 2012).

Fe^{3+}-bearing compositions $(Mg_{0.9}Fe_{0.1}Al_{0.1}Si_{0.9})O_3$ and $(Mg_{0.9}Fe_{0.2}Si_{0.9})O_3$ may exhibit a high-to-low spin transition at 55–70 GPa (Catalli *et al.* 2010b, 2011). The transition was associated with a loss of spin moment observed by X-ray emission spectroscopy, a change in Mössbauer parameters, volume collapse and decrease in compressibility at higher pressures. Other experiments showed no difference in compressibility between $MgSiO_3$ and $(Mg_{0.85}Fe_{0.15}Al_{0.15}Si_{0.85})O_3$ perovskites (Nishio-Hamane *et al.* 2008), and no discontinuities in the compression of $(Mg_{0.60}Fe^{2+}_{0.03}Fe^{3+}_{0.38}Si_{0.62}Al_{0.36})O_3$ perovskite single crystals (Boffa Ballaran *et al.* 2012). Some differences between these observations may be explained by site occupancy of Fe and Al (Caracas 2010a).

The spin transition in Fe^{3+} is expected to occur only in the Pv B-site (Hsu *et al.* 2011a), and site exchange between Fe and Al may occur only at high temperature.

In another recent experimental study, X-ray emission spectra for $(Mg_{0.75}Fe_{0.25})SiO_3$ perovskite at 80–135 GPa were typical of a mixture of high- and low-spin Fe (Mao *et al.* 2011b). This Fe^{2+}-rich perovskite was observed to be much less compressible than $MgSiO_3$ perovskite (Fig. 2). A possible explanation for elevated values of the bulk modulus seen for some studies in Fig. 2 may be incomplete relaxation of differential stress. The bulk of the experimental and theoretical data suggest that spin transitions in either Fe^{2+}- or Fe^{3+}-bearing perovskite are unlikely to cause observable anomalies in density or bulk modulus in the lower mantle.

Experimentally derived values for the bulk sound speed, V_B, at 80 GPa are shown in Fig. 2. Theoretical and most experimental studies report decreasing V_B with Fe-content. The fit to experimental data is V_B (km s^{-1}) = 10.32(5) − 1.0(1) X_{Fe}. The velocity heterogeneity parameter, $\partial \ln V_B / \partial X_{Fe}$ (Karato & Karki 2001), from experimental data is 0.10(1), in agreement with theory (0.10, Kiefer *et al.* 2002) and at the lower end of values reported for other mantle silicates (Speziale *et al.* 2005). A slightly greater decrease in V_B is observed for Fe, Al-rich compositions, but the difference is within the uncertainty. While some studies (Catalli *et al.* 2010b; Mao *et al.* 2011b) have suggested spin transitions as a possible explanation for anticorrelation of bulk and shear velocities in the deep mantle, the trends observed in most of the experimental data for Fe-bearing Pv do not support this (Fig. 2).

Ab initio theoretical studies (Kiefer *et al.* 2002; Caracas & Cohen 2005) predict the effect of Fe incorporation on both bulk and shear moduli of perovskite, allowing the seismic velocities V_P and V_S to be determined, but involve inherent approximations. The consistency between theory and experiment in bulk sound speed for (Mg,Fe)SiO_3 perovskite (Fig. 2) confirms the reliability of theoretical calculations of sound velocities at deep mantle pressures. This establishes more confidence in the application of theoretical values for not only V_B, but also V_P and V_S.

2.2 Post-perovskite

Volume compression data for (Mg,Fe)SiO_3 post-perovskite have been reported from X-ray diffraction experiments at 110–155 GPa in several studies (Fig. 3; Shieh *et al.* 2006; Guignot *et al.* 2007; Shim *et al.* 2008; Nishio-Hamane & Yagi 2009; Zhang *et al.* 2012; Dorfman *et al.* 2013). For (Mg,Fe,Al)(Fe,Al,Si)O_3 post-perovskites, data were measured from 95 to 175 GPa by Nishio-Hamane & Yagi (2009), Catalli *et al.* (2010a), Shieh *et al.* (2011) and Dorfman *et al.* (2012b). Following a similar procedure, these data were fit to equations of state to determine ρ and K and interpolated to a common reference pressure for comparison. In addition, equation of state data for perovskite compositions were extrapolated (for Fe, Al-rich perovskite, interpolated) to compare density and compressibility of these two phases. The reference pressure, 125 GPa, is near the post-perovskite transition pressure for $MgSiO_3$ (Murakami *et al.* 2004) and corresponds to ~2700 km depth, near the D″ discontinuity.

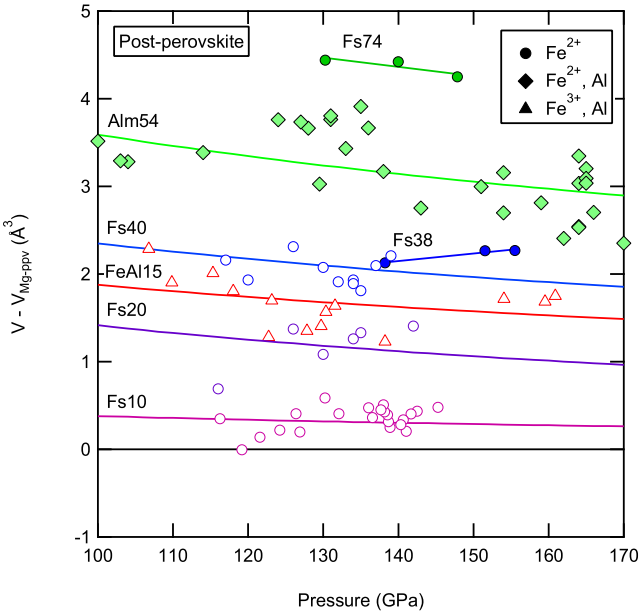

Figure 3. Volume differences between Fe- or Fe, Al-bearing post-perovskites and $MgSiO_3$ perovskite (Guignot *et al.* 2007). Fe-bearing post-perovskite with $FeSiO_3$ (Fs) from 10–74 per cent are shown in circles (Nishio-Hamane & Yagi 2009; Zhang *et al.* 2012; Dorfman *et al.* 2013). Post-perovskites synthesized from pyrope–almandine (Alm) composition with 54 per cent Alm are displayed with diamonds (Shieh *et al.* 2011). Fifteen per cent $FeAlO_3$ composition (Nishio-Hamane & Yagi 2009) is shown in triangles. Curves shown are from Birch–Murnaghan equation of state fits.

At 125 GPa, ρ is also observed to increase linearly with Fe-content in post-perovskites (Fig. 4). Post-perovskite densities are fit to the following relationship: $\rho_{125,pPv}$ (g cm^{-3}) = 5.548(1) + 1.41(3)X_{Fe}. At this pressure, the perovskite phase is less dense, but the effect of Fe-content is similar: $\rho_{125,Pv}$ (g cm^{-3}) = 5.426(11) + 1.38(4)X_{Fe}. The density difference across the post-perovskite transition, $\Delta\rho$, was measured to be 1.5 per cent (±0.1–0.7 per cent) at 125 GPa for both $MgSiO_3$ (Komabayashi *et al.* 2008) and Alm54 compositions (Shieh *et al.* 2011; Dorfman *et al.* 2012b). A comparable difference of 2.2 per cent is observed between the linear fits of the densities of perovskite and post-perovskite across the (Mg,Fe)SiO_3 join at 125 GPa (Fig. 4).

Theoretical calculations have also explored the behaviour of (Mg,Fe,Al)(Fe,Al,Si)O_3 post-perovskite at deep lower-mantle conditions (Iitaka *et al.* 2004; Caracas & Cohen 2005; Stackhouse *et al.* 2005; Wookey *et al.* 2005; Stackhouse *et al.* 2006; Tsuchiya & Tsuchiya 2006; Zhang & Oganov 2006; Caracas & Cohen 2007, 2008; Caracas 2010a,b; Hsu *et al.* 2012; Yu *et al.* 2012). These predictions have used LDA and GGA methods, and more recently, Hubbard U corrections to better model the electronic spin state of Fe. Calculated densities for the perovskite and post-perovskite phases at 125–136 GPa are in good agreement with experimental measurements at 125 GPa, though they yield a lower density contrast between the two phases for Fe-rich compositions: $\Delta\rho$ is 1.4 per cent for $MgSiO_3$ but only 0.5–1.1 per cent for $FeSiO_3$ (Caracas & Cohen 2005; Wookey *et al.* 2005; Stackhouse *et al.* 2006). The slope of increase in ρ_{125} with X_{Fe} from LDA calculations is in better agreement with experimental data than GGA, which underestimates the effect of Fe. No significant difference was predicted between the densities of Fe^{2+}- and Fe^{3+}-bearing post-perovskite (Yu *et al.* 2012).

The bulk modulus of the post-perovskite phase was found to be more compressible with higher Fe-content (Zhang *et al.* 2012, Fig. 4) and this can be described by: $K_{125,pPv}$ (GPa) = 665(3) − 81(16)X_{Fe}. In contrast, data for the perovskite phase at this pressure show no significant change in bulk modulus with Fe-content. The fit to $K_{125,Pv}$ for perovskites is 692(7) GPa + 30(52) GPa × X_{Fe}. Experimental trends thus show increasing contrast in V_B between Pv and pPv with Fe-content (Fig. 4). From X_{Fe} = 0 to 40, the contrast in bulk sound speed between perovskite and post-perovskite phases more than doubles, from 3.1 to 6.4 per cent. This increase in contrast in $V_{B,Pv} - V_{B,pPv}$ is not reported in theoretical studies, which predict only a slight effect of Fe-content on $K_{125,pPv}$ (Fig. 4).

Volume compression data observed by Shieh *et al.* (2011) for $((Mg,Fe)_{0.75}Al_{0.25})(Al_{0.25}Si_{0.75})O_3$ post-perovskites suggest a strong increase in bulk modulus for more Fe-rich post-perovskite, but additional data are needed to confirm this (Shieh *et al.* 2011). Although data for Fe#74 post-perovskite observed by Dorfman *et al.* (2013) are insufficient to determine bulk modulus, they also indicate higher volumes than predicted by the trend in Zhang *et al.* (2012). Possible mechanisms for an increase in bulk modulus for compositions with Fe#>40 could include a spin transition (e.g. Lin *et al.* 2008) or a

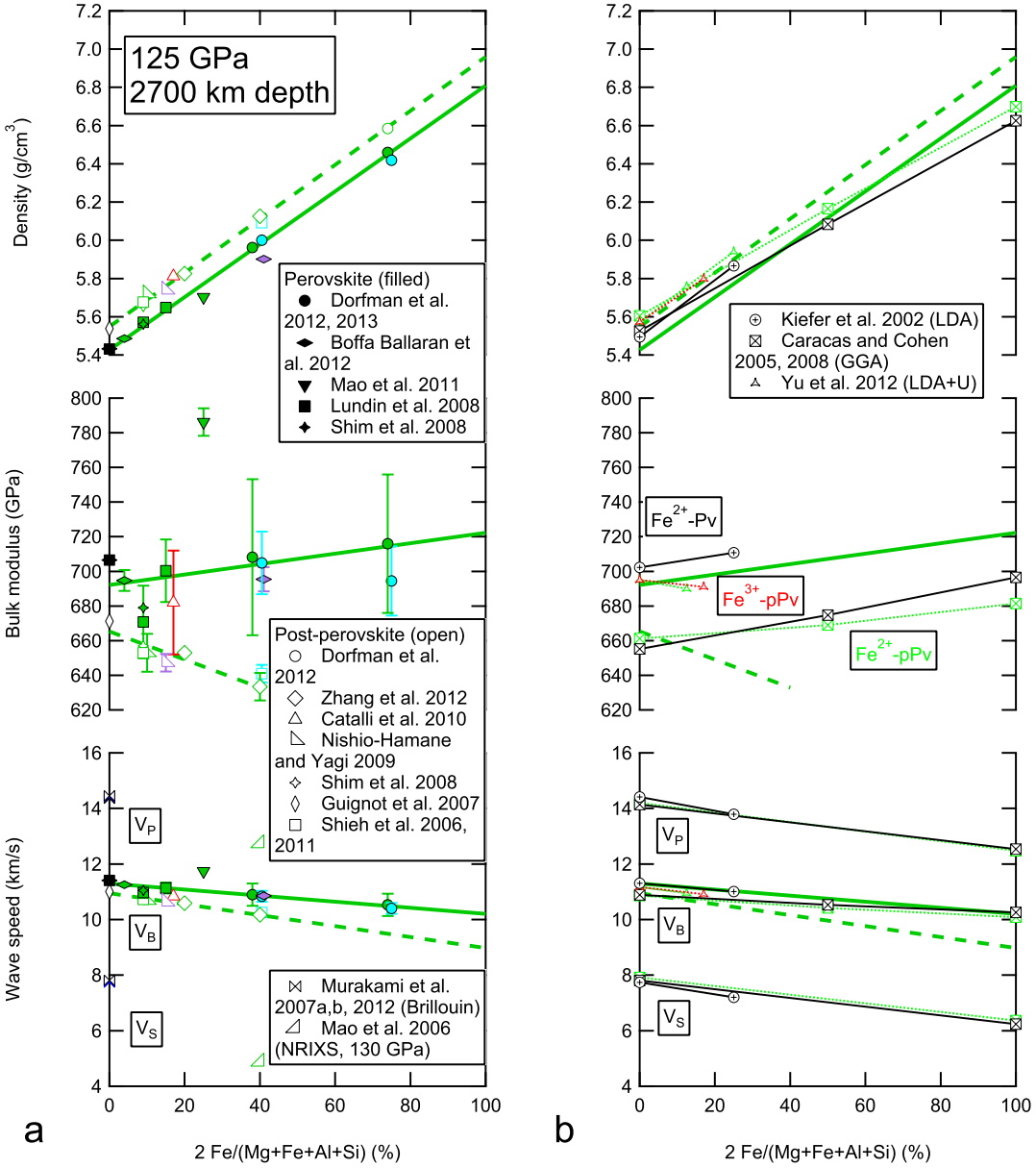

Figure 4. (a) At 125 GPa and 300 K, density, bulk modulus and seismic wave propagation speeds for perovskites and post-perovskites with varying Fe, Al-content determined from experimental data (Mao *et al.* 2006; Shieh *et al.* 2006; Guignot *et al.* 2007; Murakami *et al.* 2007b, 2007a; Lundin *et al.* 2008; Shim *et al.* 2008; Nishio-Hamane & Yagi 2009; Cataldi *et al.* 2010a; Mao *et al.* 2011b; Shieh *et al.* 2011; Boffa Ballaran *et al.* 2012; Dorfman *et al.* 2012b; Zhang *et al.* 2012; Dorfman *et al.* 2013). Colors of symbols have same meanings as in Fig. 2. Bold green line fits are shown to Fe^{2+}-bearing compositions (solid = perovskite, dashed = post-perovskite). (b) Density functional theory results at 125 GPa and 0 K for $(Mg,Fe)SiO_3$ perovskites and post-perovskites from LDA (Kiefer *et al.* 2002; Yu *et al.* 2012) and GGA (Caracas & Cohen 2005, 2008). Perovskite calculations are shown in solid black. Post-perovskite results are dotted and shown in green for Fe^{2+}-bearing compositions, while dotted red represent Fe^{3+}-bearing compositions.

modification of the post-perovskite structure in Fe-rich compositions (Yamanaka *et al.* 2010).

A large decrease in shear modulus with Fe-content in post-perovskite was observed in a nuclear resonant inelastic X-ray scattering experiment by Mao *et al.* (2006). Based on measured partial phonon density of states of Fe and volume compression data, this experiment determined velocities V_P and V_S of an $(Mg_{0.6}Fe_{0.4})SiO_3$ pPv lower than those of $MgSiO_3$ pPv by 11 and 38 per cent, respectively (Fig. 4). However, this technique is sensitive to the extrapolation from the partial phonon density of states which may lead to underestimation of velocities (Sturhahn & Jackson 2007). This has been the only experimental determination of bulk elastic wave velocities of an Fe-bearing silicate at deep mantle pressures.

Theoretical studies do not predict any stiffening of the bulk modulus or large decrease in elastic wave velocities at high Fe-content. A spin transition in post-perovskite was not predicted to occur at Earth-relevant pressures (Caracas & Cohen 2008). Overall, given the higher required experimental pressures and more limited data, it is perhaps not surprising that the observed variation in pPv properties with Fe-content is more uncertain and less consistent with theory. Further compression experiments on Fe-rich pPv are needed at deep lower-mantle pressures.

3 IMPLICATIONS FOR MANTLE HETEROGENEITIES

The volume or density is the property most precisely constrained by the experiments discussed above and is the driver of thermochemical convection in the mantle. The style of convection will depend on the relative contributions of chemical and thermal anomalies (Davaille 1999; Deschamps & Tackley 2008). A fundamental question is whether dense chemical heterogeneities are entrained in mantle convection or sequestered at the core–mantle boundary. To remain at the core–mantle boundary, chemical heterogeneities must be enriched enough in heavy elements (Fe) to offset thermal buoyancy. Assuming thermal and chemical effects are independent (Anderson & Hama 1999), for a hot, dense heterogeneity with neutral buoyancy, the thermal and chemical effects are equal:

$$-\alpha\rho\Delta T = \frac{\partial\rho}{\partial X_{\mathrm{Fe}}}\Delta X_{\mathrm{Fe}}. \quad (1)$$

Using the experimental results discussed above, we can calculate the Fe-enrichment necessary to balance thermal anomalies. The variation of thermal expansivity, α, with pressure and temperature for $MgSiO_3$ was estimated from density functional theory calculations (Wentzcovitch *et al.* 2004) yielding $\alpha\rho = 7.63 \times 10^{-5}$ g cm^{-3}/K for $MgSiO_3$ perovskite at 80 GPa and 2000 K. The difference in density due to temperature relative to that of end-member $MgSiO_3$ perovskite at 2000 K and 80 GPa was calculated for temperature anomalies of 200, 500 and 800 K (Fig. 5a). Based on the effect of Fe-content on density at this pressure (Fig. 2), a chemical heterogeneity with Mg# (Mg/(Mg+Fe)) = 87 would be neutrally buoyant in a Mg# 90 mantle if it is also 500 K hotter than the surrounding rock (Fig. 5b). This is consistent with long-term stability of dense heterogeneities in the deep mantle estimated by probabilistic tomography to be enriched in Fe by 2 per cent and warmer by 300 K (Trampert *et al.* 2004).

Based on current experimental data, the density contrast between perovskite and post-perovskite phases appears to be insensitive to temperature (Komabayashi *et al.* 2008) and Fe-content. Komabayashi *et al.* (2008) observed that the 1.5 per cent density contrast across the post-perovskite transition would be equivalent to the contrast due to a 1300 K difference in temperature. The 2.2 per cent density contrast shown by our $(Mg,Fe)SiO_3$ perovskite and post-perovskite data set may imply an even greater impact of the post-perovskite transition on buoyancy (equivalent to a 1900 K thermal difference). This density contrast could also be produced in either silicate phase at 125 GPa by a ΔX_{Fe} of 9 Mg# (Mg# 81, relative to Mg#90, see Fig. 4). However, both Fe and Al contents have strong effects on the pressure and width of the post-perovskite transition, so the depth at which this density difference is observed and its sharpness will depend on composition. In Fe-rich compositions, a broad post-perovskite transition has been observed with a mixture of very Fe-rich post-perovskite and Fe-poor perovskite (Mao *et al.* 2004, 2005; Dorfman *et al.* 2013). A two-phase loop with difference in Fe-content between post-perovskite and perovskite $X_{\mathrm{Fe},pPv} - X_{\mathrm{Fe},Pv}$ as high as 0.6 (Dorfman *et al.* 2013) would have a high contrast in properties between these two phases at the base of the lower mantle: $\Delta\rho$ between adjacent perovskite and post-perovskite grains could be up to ~0.8 g cm^{-3}, or 13 per cent. This contrast could have important implications for the rheology of the D″ phase assemblage (Ammann *et al.* 2010).

The effect of Fe-incorporation on density of perovskite and post-perovskite can be used to determine composition of heterogeneities. Recent studies have suggested that observed lower-mantle densities (Ricolleau *et al.* 2009) and shear wave velocities (Murakami *et al.* 2012) are consistent with a Si-enriched composition, at least 93 per cent perovskite. Assuming a perovskitic lower mantle, density contrasts may be dominated by differences in Fe-content in perovskite or post-perovskite. Based on the trend in Fig. 2, an LLSVP with density up to 2–5 per cent greater than a Mg/(Mg+Fe) 90 per cent bulk mantle would be consistent with Mg/(Mg+Fe) of as low as 78–88 per cent in perovskite. A ULVZ at the core–mantle boundary 10 per cent denser than Mg#90 post-perovskite could be composed of Mg#50 post-perovskite. Based on theoretical (Wookey *et al.* 2005; Stackhouse *et al.* 2006; Caracas & Cohen 2008) and experimental (Mao *et al.* 2006) constraints on V_{P}, Mg#50 post-perovskite would propagate P waves ~6–20 per cent slower than Mg#90 post-perovskite, similar to the 4–19 per cent V_{P} reduction observed by Rost & Garnero (2006). A $FeSiO_3$ post-perovskite would be 22 per cent denser than Mg#90. If regions are observed with greater density than this (e.g. Rost & Garnero 2006), they

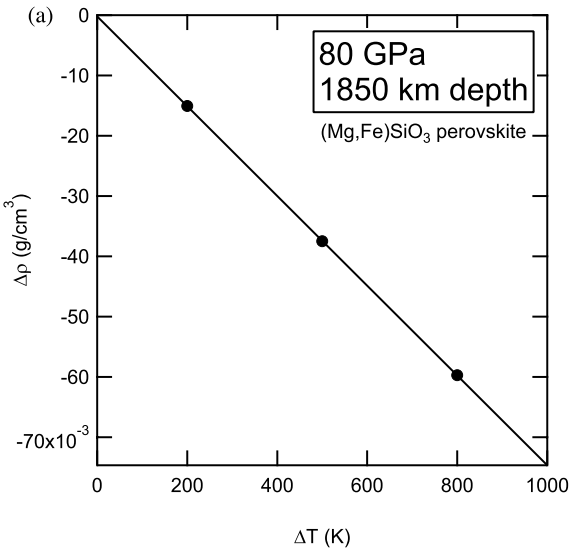

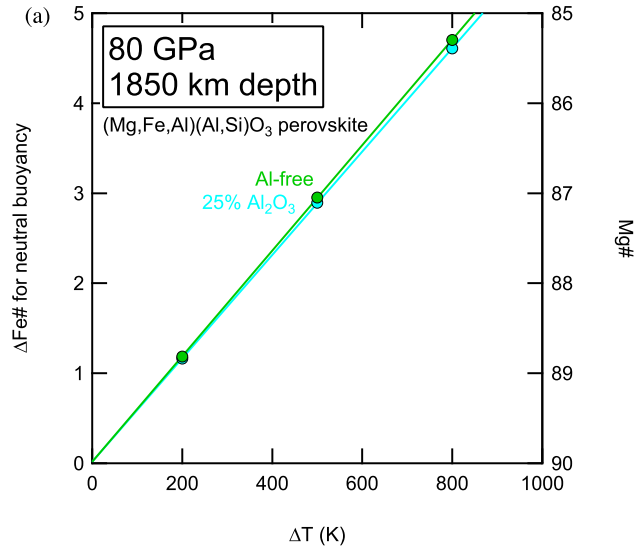

Figure 5. (a) Effect of 200, 500 and 800 K thermal anomalies on density of perovskite from Wentzcovitch *et al.* (2004). (b) From density data for Fe-rich and Fe, Al-rich perovskites, amount of Fe-enrichment necessary to balance buoyancy due to temperature.

must be both richer in Fe and poorer in Si, that is, enriched in denser (Mg,Fe)O or Fe metal.

For compositions with more (Mg,Fe)O or other Si- or Al-rich phases, we must also consider the effects of these phases on chemical partitioning and phase equilibria. Ricolleau *et al.* (2009) observed that the partitioning of Fe between (Mg,Fe)O and silicate phases has a negligible effect on the density of the mantle. Similar modelling with our data set shows that varying the partitioning coefficient, K_D, of Fe between perovskite and magnesiowüstite over the range of experimental values (e.g. Auzende *et al.* 2008; Sakai *et al.* 2009) results in density differences of 0.1 per cent. Exchange of Fe with (Mg,Fe)O may have more important effects on the depth and sharpness of the post-perovskite transition (Grocholski *et al.* 2012). In the (Mg,Fe)SiO_3 system, Fe-incorporation was observed to produce a shallower and broader phase transition (e.g. Dorfman *et al.* 2013), but partitioning of Fe into the oxide phase sharpens the transition. Al incorporation has been observed to deepen and broaden the post-perovskite transition such that Al-rich post-perovskite would not be observed in the lower mantle (Tateno *et al.* 2005; Dorfman *et al.* 2012b). Stabilization of perovskite in Fe, Al-rich heterogeneities could possibly produce anticorrelated V_B and V_S due to the 3–7 per cent higher V_B observed in perovskite relative to post-perovskite of the same composition (at 125 GPa, Fig. 4). However, in compositions with sufficiently high Si, Al-content such as MORB, the presence of separate Si- and Al-bearing phases erased this effect on the post-perovskite transition (Grocholski *et al.* 2012).

In summary, experimental and theoretical data are compiled to determine the effects of Fe and/or Al incorporation on the elastic properties of (Mg,Fe,Al)(Fe,Al,Si)O_3 perovskite and post-perovskite at representative mantle depths. Using recent volume compression data on perovskites with up to 75 per cent $FeSiO_3$, we provide constraints on the density, bulk modulus and bulk sound speed of Fe-bearing perovskites. Experimental compression data for perovskite are in good agreement with density functional theory calculations, showing a weak increase in the bulk modulus with Fe-content. For post-perovskite, experimental studies have observed a decrease in bulk modulus with Fe-content, in contrast to theory. Electronic spin transitions and differences in valence state of Fe in perovskite and post-perovskite phases are not expected to produce observable differences in seismic velocities in the lower mantle. Across the post-perovskite transition, the experimental data show a density increase of ∼2 per cent and an increasing contrast in bulk compressibility with Fe-content. The density contrast across the phase transition is comparable to the contrast due to decreasing Mg# by 9 or decreasing temperature by 1900 K. Al may increase the density of Fe-bearing perovskite by allowing paired substitution for Mg and Si, but can stabilize perovskite over post-perovskite.

ACKNOWLEDGEMENTS

The National Science Foundation and Carnegie-Department of Energy Alliance Center provided support for this research.

REFERENCES

Ammann, M.W., Brodholt, J.P., Wookey, J. & Dobson, D.P., 2010. First-principles constraints on diffusion in lower-mantle minerals and a weak D" layer, *Nature,* **465**(7297), 462–465.

Anderson, O.L. & Hama, J., 1999. Shifts in thermal expansivity with Fe content for solid solutions of $MgSiO_3$–$FeSiO_3$ with the perovskite structure, *Am. Mineral.,* **84**(3), 221–225.

Andrault, D., Bolfan-Casanova, N., Bouhifd, M.A., Guignot, N. & Kawamoto, T., 2007. The role of Al-defects on the equation of state of Al-(Mg,Fe)SiO_3 perovskite, *Earth planet. Sci. Lett.,* **263**(3–4), 167–179.

Auzende, A., Badro, J., Ryerson, F.J., Weber, P.K., Fallon, S.J., Addad, A., Siebert, J. & Fiquet, G., 2008. Element partitioning between magnesium silicate perovskite and ferropericlase: new insights into bulk lower mantle geochemistry, *Earth planet. Sci. Lett.,* **269,** 164–174.

Badro, J., Rueff, J., Vanko, G., Monaco, G., Fiquet, G. & Guyot, F., 2004. Electronic transitions in perovskite: possible nonconvecting layers in the lower mantle, *Science,* **305**(5682), 383–386.

Bengtson, A., Persson, K. & Morgan, D., 2007. Ab initio study of the composition dependence of the pressure-induced spin crossover in perovskite (Mg_{1-x},Fe_x)SiO_3, *Earth planet. Sci. Lett.,* **265,** 535–545.

Birch, F., 1947. Finite elastic strain of cubic crystals, *Phys. Rev.,* **71**(11), 809–824.

Boffa Ballaran, T.B., Kurnosov, A., Glazyrin, K., Frost, D.J., Merlini, M., Hanfland, M. & Caracas, R., 2012. Effect of chemistry on the compressibility of silicate perovskite in the lower mantle, *Earth planet. Sci. Lett.,* **333–334,** 181–190.

Brodholt, J.P., 2000. Pressure-induced changes in the compression mechanism of aluminous perovskite in the Earth's mantle, *Nature,* **407,** 620–622.

Caracas, R., 2010a. Elasticity of $AlFeO_3$ and $FeAlO_3$ perovskite and post-perovskite from first-principles calculations, *Geophys. Res. Lett.,* **37,** L20306, doi:10.1029/2010GL044404.

Caracas, R., 2010b. Spin and structural transitions in $AlFeO_3$ and $FeAlO_3$ perovskite and post-perovskite, *Phys. Earth planet. Inter*. **182,** 10–17.

Caracas, R. & Cohen, R., 2007. Effect of chemistry on the physical properties of perovskite and post-perovskite, in *Post-Perovskite: The Last Mantle Phase Transition,* vol. 174 of Geophysical Monograph Series, pp. 115–128, American Geophysical Union, Washington, DC.

Caracas, R. & Cohen, R.E., 2005. Effect of chemistry on the stability and elasticity of the perovskite and post-perovskite phases in the $MgSiO_3$–$FeSiO_3$–Al_2O_3 system and implications for the lowermost mantle, *Geophys. Res. Lett.,* **32,** L16310, doi: 10.1029/2005GL023164.

Caracas, R. & Cohen, R.E., 2008. Ferrous iron in post-perovskite from first-principles calculations, *Phys. Earth planet. Inter.,* **168**(3–4), 147–152.

Caracas, R., Mainprice, D. & Thomas, C., 2010. Is the spin transition in Fe^{2+}-bearing perovskite visible in seismology? *Geophys. Res. Lett.,* **37,** L13309, doi:10.1029/2010GL043320.

Catalli, K., Shim, S.-H., Prakapenka, V.B., Zhao, J. & Sturhahn, W., 2010a. X-ray diffraction and Mössbauer spectroscopy of Fe^{3+}-bearing Mg-silicate post-perovskite at 128-138 GPa, *Am. Mineral.,* **95**(2–3), 418–421.

Catalli, K. *et al.*, 2010b. Spin state of ferric iron in $MgSiO_3$ perovskite and its effect on elastic properties, *Earth planet. Sci. Lett.,* **289**(1–2), 68–75.

Catalli, K. *et al.*, 2011. Effects of the Fe^{3+} spin transition on the properties of aluminous perovskite and new insights for lower-mantle seismic heterogeneities, *Earth planet. Sci. Lett.,* **310**(3–4), 293–302.

Davaille, A., 1999. Simultaneous generation of hotspots and superswells by convection in a heterogeneous planetary mantle, *Nature,* **402**(6763), 756–760.

Deschamps, F. & Tackley, P., 2008. Searching for models of thermo-chemical convection that explain probabilistic tomography: I. Principles and influence of rheological parameters, *Phys. Earth planet. Inter.,* **171**(1–4), 357–373.

Dewaele, A., Loubeyre, P. & Mezouar, M., 2004. Equations of state of six metals above 94 GPa, *Phys. Rev. B,* **70**(9), 094112.

Dobson, D.P. & Brodholt, J.P., 2005. Subducted banded iron formations as a source of ultralow-velocity zones at the core-mantle boundary, *Nature,* **434**(7031), 371–374.

Dorfman, S.M., Meng, Y., Prakpenka, V.B. & Duffy, T.S., 2013. Effects of Fe-enrichment on the equation of state and stability of (Mg,Fe)SiO_3 perovskite, *Earth planet. Sci. Lett.,* **361,** 249–257.

Dorfman, S.M., Prakapenka, V.B., Meng, Y. & Duffy, T.S., 2012a. Intercomparison of pressure standards (Au, Pt, Mo, MgO, NaCl and Ne) to 2.5 Mbar, *J. geophys. Res.,* **117**, B08210, doi: 10.1029/2012JB009292.

Dorfman, S.M., Shieh, S.R., Meng, Y., Prakapenka, V.B. & Duffy, T.S., 2012b. Synthesis and equation of state of perovskites in the $(Mg,Fe)_3Al_2Si_3O_{12}$ system to 177 GPa, *Earth planet. Sci. Lett.,* **357–358,** 194–202.

Duffy, T.S., 2005. Synchrotron facilities and the study of the Earth's deep interior, *Rep. Prog. Phys.,* **68,** 1811–1859.

Fei, Y., Ricolleau, A., Frank, M., Mibe, K., Shen, G. & Prakapenka, V.B., 2007. Toward an internally consistent pressure scale, *Proc. Natl. Acad. Sci.,* **104**(22), 9182–9186.

Frost, D.J. & Langenhorst, F., 2002. The effect of Al_2O_3 on Fe–Mg partitioning between magnesiowüstite and magnesium silicate perovskite, *Earth planet. Sci. Lett.,* **199,** 227–241.

Garnero, E.J., 2000. Heterogeneity of the lowermost mantle, *Annu. Rev. Earth planet. Sci.,* **28**(1), 509–537.

Garnero, E.J. & Helmberger, D.V., 1995. A very slow basal layer underlying large-scale low-velocity anomalies in the lower mantle beneath the Pacific: evidence from core phases, *Phys. Earth planet. Inter.,* **91**(1–3), 161–176.

Grocholski, B., Catalli, K., Shim, S.-H. & Prakapenka, V., 2012. Mineralogical effects on the detectability of the postperovskite boundary, *Proc. Natl. Acad. Sci.,* **109,** 2275–2279.

Guignot, N., Andrault, D., Morard, G., Bolfan-Casanova, N. & Mezouar, M., 2007. Thermoelastic properties of post-perovskite phase $MgSiO_3$ determined experimentally at core-mantle boundary P-T conditions, *Earth planet. Sci. Lett.,* **256**(1–2), 162–168.

Hsu, H., Blaha, P., Cococcioni, M. & Wentzcovitch, R.M., 2011a. Spin-state crossover and hyperfine interactions of ferric iron in $(Mg,Fe)SiO_3$ perovskite, *Phys. Rev. Lett.,* **106**(11), 118501.

Hsu, H., Umemoto, K., Blaha, P. & Wentzcovitch, R.M., 2010. Spin states and hyperfine interactions of iron in $(Mg,Fe)SiO_3$ perovskite under pressure, *Earth planet. Sci. Lett.,* **294**(1–2), 19–26.

Hsu, H., Umemoto, K., Cococcioni, M. & Wentzcovitch, R.M., 2011b. The Hubbard U correction for iron-bearing minerals: a discussion based on $(Mg,Fe)SiO_3$ perovskite, *Phys. Earth planet. Inter.,* **185**(1–2), 13–19.

Hsu, H., Yu, Y.G. & Wentzcovitch, R.M., 2012. Spin crossover of iron in aluminous $MgSiO_3$ perovskite and post-perovskite, *Earth planet. Sci. Lett.,* **359–360,** 34–39.

Huang, D. & Pan, Y., 2012. Pressure-induced spin transitions of iron in $MgSiO_3$ perovskite: a GGA+U study, *High Press. Res.,* **32**(2), 270–279.

Hutko, A.R., Lay, T., Garnero, E.J. & Revenaugh, J., 2006. Seismic detection of folded, subducted lithosphere at the core-mantle boundary, *Nature,* **441**(7091), 333–336.

Iitaka, T., Hirose, K., Kawamura, K. & Murakami, M., 2004. The elasticity of the $MgSiO_3$ post-perovskite phase in the Earth's lowermost mantle, *Nature,* **430**(6998), 442–445.

Irifune, T., Koizumi, T. & Ando, J., 1996. An experimental study of the garnet-perovskite transformation in the system $MgSiO_3$–$Mg_3Al_2Si_3O_{12}$, *Phys. Earth planet. Inter.,* **96,** 147–157.

Ishii, M. & Tromp, J., 1999. Normal-mode and free-air gravity constraints on lateral variations in velocity and density of Earth's mantle, *Science,* **285**(5431), 1231–1236.

Jackson, I., 1998. Elasticity, composition and temperature of the Earth's lower mantle: a reappraisal, *Geophys. J. Int.,* **134**(1), 291–311.

Jackson, J.M., Sturhahn, W., Shen, G., Zhao, J., Hu, M.Y., Errandonea, D., Bass, J.D. & Fei, Y., 2005. A synchrotron Mössbauer spectroscopy study of $(Mg,Fe)SiO_3$ perovskite up to 120 GPa, *Am. Mineral.,* **90,** 199–205.

Karato, S. & Karki, B.B., 2001. Origin of lateral variation of seismic wave velocities and density in the deep mantle, *J. geophys. Res.,* **106**(B10), 21 771–21 783.

Karki, B.B., Wentzcovitch, R.M., de Gironcoli, S. & Baroni, S., 2001. First principles thermoelasticity of $MgSiO_3$-perovskite: consequences for the inferred properties of the lower mantle, *Geophys. Res. Lett,* **28**(14), 2699–2702.

Kiefer, B., Stixrude, L. & Wentzcovitch, R.M., 2002. Elasticity of $(Mg,Fe)SiO_3$-perovskite at high pressures, *Geophys. Res. Lett.,* **29**(11), 34-1–34-4.

Knittle, E. & Jeanloz, R., 1989. Simulating the core-mantle boundary: an experimental study of high-pressure reactions between silicates and liquid iron, *Geophys. Res. Lett.,* **16**(7), 609–612.

Knittle, E. & Jeanloz, R., 1991. Earth's core-mantle boundary: results of experiments at high pressures and temperatures, *Science,* **251**(5000), 1438–1443.

Komabayashi, T., Hirose, K., Sugimura, E., Sata, N., Ohishi, Y. & Dubrovinsky, L.S., 2008. Simultaneous volume measurements of post-perovskite and perovskite in $MgSiO_3$ and their thermal equations of state, *Earth planet. Sci. Lett.,* **265**(3–4), 515–524.

Labrosse, S., Hernlund, J.W. & Coltice, N., 2007. A crystallizing dense magma ocean at the base of the Earth's mantle, *Nature,* **450**(7171), 866–869.

Li, J. *et al.*, 2004. Electronic spin state of iron in lower mantle perovskite, *Proc. Natl. Acad. Sci.,* **101**(39), 14 027–14 030.

Li, L., Brodholt, J.P., Stackhouse, S., Weidner, D.J., Alfredsson, M. & Price, G.D., 2005. Elasticity of $(Mg,Fe)(Si,Al)O_3$-perovskite at high pressure, *Earth planet. Sci. Lett.,* **240**(2), 529–536.

Lin, J.-F. *et al.*, 2008. Intermediate-spin ferrous iron in lowermost mantle post-perovskite and perovskite, *Nat. Geosci.,* **1**(10), 688–691.

Lin, J.-F., Speziale, S., Mao, Z. & Marquardt, H., 2013. Effects of the electronic spin transitions of iron in lower mantle minerals: implications for deep mantle geophysics and geochemistry, *Rev. Geophys.,* **51,** 244–275.

Lundin, S., Catalli, K., Santillan, J., Shim, S.-H., Prakapenka, V.B., Kunz, M. & Meng, Y., 2008. Effect of Fe on the equation of state of mantle silicate perovskite over 1 Mbar, *Phys. Earth planet. Inter.,* **168,** 97–102.

Mao, W.L. *et al.*, 2004. Ferromagnesian postperovskite silicates in the D" layer of the Earth, *Proc. Natl. Acad. Sci. U.S.A.,* **101**(45), 15 867–15 869.

Mao, W.L. *et al.*, 2005. Iron-rich silicates in the Earth's D" layer, *Proc. Natl. Acad. Sci.,* **102**(28), 9751–9753.

Mao, W.L. *et al.*, 2006. Iron-rich post-perovskite and the origin of ultralow-velocity zones, *Science,* **312**(5773), 564–565.

Mao, Z., Jacobsen, S.D., Frost, D.J., McCammon, C.A., Hauri, E.H. & Duffy, T.S., 2011a. Effect of hydration on the single-crystal elasticity of Fe-bearing wadsleyite to 12 GPa, *Am. Mineral.,* **96**(10), 1606–1612.

Mao, Z., Lin, J., Scott, H., Watson, H., Prakapenka, V., Xiao, Y., Chow, P. & McCammon, C., 2011b. Iron-rich perovskite in the Earth's lower mantle, *Earth planet. Sci. Lett.,* **309,** 179–184.

Masters, G., Laske, G., Bolton, H. & Dziewonski, A., 2000. The relative behavior of shear velocity, bulk sound speed, and compressional velocity in the mantle: implications for chemical and thermal structure, in *Earth's Deep Interior: Mineral Physics and Tomography from the Atomic to the Global Scale,* pp. 63–87, ed. Karato, S., American Geophysical Union, Washington, DC.

Mattern, E., Matas, J., Ricard, Y. & Bass, J., 2005. Lower mantle composition and temperature from mineral physics and thermodynamic modelling, *Geophys. J. Int.,* **160**(3), 973–990.

McCammon, C. *et al.*, 2008. Stable intermediate-spin ferrous iron in lower-mantle perovskite, *Nat. Geosci.,* **1**(10), 684–687.

McCammon, C.A., 1997. Perovskite as a possible sink for ferric iron in the lower mantle, *Nature,* **387,** 694–696.

McCammon, C.A., Dubrovinsky, L., Narygina, O., Kantor, I., Wu, X., Glazyrin, K., Sergueev, I. & Chumakov, A., 2010. Low-spin Fe^{2+} in silicate perovskite and a possible layer at the base of the lower mantle, *Phys. Earth planet. Inter.,* **180**(3–4), 215–221.

McNamara, A.K. & Zhong, S., 2004. Thermochemical structures within a spherical mantle: superplumes or piles? *J. geophys. Res.,* **109,** doi:10.1029/2003JB002847.

McNamara, A.K. & Zhong, S., 2005. Thermochemical structures beneath Africa and the Pacific Ocean, *Nature,* **437**(7062), 1136–1139.

Metsue, A. & Tsuchiya, T., 2012. Thermodynamic properties of $(Mg,Fe^{2+})SiO_3$ perovskite at the lower-mantle pressures and temperatures: an internally consistent LSDA+U study, *Geophys. J. Int.,* **190**(1), 310–322.

Murakami, M., Hirose, K., Kawamura, K., Sata, N. & Ohishi, Y., 2004. Post-perovskite phase transition in $MgSiO_3$, *Science,* **304**(5672), 855–858.

Murakami, M., Ohishi, Y., Hirao, N. & Hirose, K., 2012. A perovskitic lower mantle inferred from high-pressure, high-temperature sound velocity data, *Nature,* **485**(7396), 90–94.

Murakami, M., Sinogeikin, S.V., Bass, J.D., Sata, N., Ohishi, Y. & Hirose, K., 2007a. Sound velocity of $MgSiO_3$ post-perovskite phase: a constraint on the D" discontinuity, *Earth planet. Sci. Lett.,* **259**(1–2), 18–23.

Murakami, M., Sinogeikin, S.V., Hellwig, H., Bass, J.D. & Li, J., 2007b. Sound velocity of $MgSiO_3$ perovskite to Mbar pressure, *Earth planet. Sci. Lett.,* **256**(1–2), 47–54.

Nakagawa, T., Tackley, P.J., Deschamps, F. & Connolly, J.A., 2012. Radial 1-D seismic structures in the deep mantle in mantle convection simulations with self-consistently calculated mineralogy, *Geochem. Geophys. Geosyst.,* **13**(11), doi:10.1029/2012GC004325.

Nishio-Hamane, D., Seto, Y., Fujino, K. & Nagai, T., 2008. Effect of $FeAlO_3$ incorporation into $MgSiO_3$ perovskite on the bulk modulus of perovskite, *Phys. Earth planet. Inter.,* **166,** 219–225.

Nishio-Hamane, D. & Yagi, T., 2009. Equations of state for postperovskite phases in the $MgSiO_3$–$FeSiO_3$–$FeAlO_3$ system, *Phys. Earth planet. Inter.,* **175**(3–4), 145–150.

Oganov, A.R. & Ono, S., 2004. Theoretical and experimental evidence for a post-perovskite phase of $MgSiO_3$ in Earth's D" layer, *Nature,* **430**(6998), 445–448.

Ricolleau, A. *et al.*, 2009. Density profile of pyrolite under the lower mantle conditions, *Geophys. Res. Lett.,* **36**(6), L06302, doi:10.1029/2008GL036759.

Rost, S. & Garnero, E.J., 2006. Detection of an ultralow velocity zone at the core-mantle boundary using diffracted PKKPab waves, *J. geophys. Res.,* **111,** B07309, doi:10.1029/2005JB003850.

Saikia, A., Boffa Ballaran, T.B. & Frost, D.J., 2009. The effect of Fe and Al substitution on the compressibility of $MgSiO_3$-perovskite determined through single-crystal X-ray diffraction, *Phys. Earth planet. Inter.,* **173**(1–2), 153–161.

Sakai, T. *et al.*, 2009. Fe-Mg partitioning between perovskite and ferropericlase in the lower mantle, *Am. Mineral.,* **94**(7), 921–925.

Shieh, S.R., Dorfman, S.M., Kubo, A., Prakapenka, V.B. & Duffy, T.S., 2011. Synthesis and equation of state of post-perovskites in the $(Mg,Fe)_3Al_2Si_3O_{12}$ system, *Earth planet. Sci. Lett.,* **312,** 422–428.

Shieh, S.R., Duffy, T.S., Kubo, A., Shen, G., Prakapenka, V.B., Sata, N., Hirose, K. & Ohishi, Y., 2006. Equation of state of the postperovskite phase synthesized from a natural $(Mg,Fe)SiO_3$ orthopyroxene, *Proc. Natl. Acad. Sci. U.S.A.,* **103**(9), 3039–3043.

Shim, S.-H., Catalli, K., Hustoft, J., Kubo, A., Prakapenka, V.B., Caldwell, W.A. & Kunz, M., 2008. Crystal structure and thermoelastic properties of $(Mg_{0.91}\ Fe_{0.09})SiO_3$ postperovskite up to 135 GPa and 2,700 K, *Proc. Natl. Acad. Sci.,* **27,** 7382–7386.

Sinmyo, R., Ozawa, H., Hirose, K., Yasuhara, A., Endo, N., Sata, N. & Ohishi, Y., 2008. Ferric iron content in $(Mg,Fe)SiO_3$ perovskite and post-perovskite at deep lower mantle conditions, *Am. Mineral.,* **93**(11–12), 1899–1902.

Sinmyo, R., Hirose, K., Muto, S., Ohishi, Y. & Yasuhara, A., 2011. The valence state and partitioning of iron in the Earth's lowermost mantle, *J. geophys. Res.,* **116,** B07205, doi:10.1029/2010JB008179.

Speziale, S., Jiang, F. & Duffy, T.S., 2005. Compositional dependence of the elastic wave velocities of mantle minerals: implications for seismic properties of mantle rocks, in *Earth's Deep Mantle: Structure, Composition, and Evolution,* vol. 160 of Geophysical Monograph Series, pp. 301–320, eds van der Hilst, R.D., Bass, J.D., Matas, J. & Trampert, J., American Geophysical Union, Washington, DC.

Stackhouse, S., Brodholt, J.P., Wookey, J., Kendall, J. & Price, G.D., 2005. The effect of temperature on the seismic anisotropy of the perovskite and post-perovskite polymorphs of $MgSiO_3$, *Earth planet. Sci. Lett.,* **230**(1–2), 1–10.

Stackhouse, S., Brodholt, J.P. & Price, G.D., 2006. Elastic anisotropy of $FeSiO_3$ end-members of the perovskite and post-perovskite phases, *Geophys. Res. Lett.,* **33,** L01304, doi:10.1029/2005GL023887.

Stixrude, L. & Lithgow-Bertelloni, C., 2012. Geophysics of chemical heterogeneity in the mantle, *Annu. Rev. Earth planet. Sci.,* **40**(1), 569–595.

Sturhahn, W. & Jackson, J., 2007. Geophysical applications of nuclear resonant spectroscopy, *GSA Special Papers,* **421,** 157–174.

Tange, Y., Takahashi, E., Nishihara, Y., Funakoshi, K. & Sata, N., 2009. Phase relations in the system MgO-FeO-SiO_2 to 50 GPa and 2000°C: an application of experimental techniques using multianvil apparatus with sintered diamond anvils, *J. geophys. Res.,* **114,** B02214, doi:10.1029/2008JB005891.

Tateno, S., Hirose, K., Sata, N. & Ohishi, Y., 2005. Phase relations in $Mg_3Al_2Si_3O_{12}$ to 180 GPa: effect of Al on post-perovskite phase transition, *Geophys. Res. Lett.,* **32,** L15306, doi:10.1029/2005GL023309.

Trampert, J., Deschamps, F., Resovsky, J. & Yuen, D., 2004. Probabilistic tomography maps chemical heterogeneities throughout the lower mantle, *Science,* **306**(5697), 853–856.

Trampert, J., Vacher, P. & Vlaar, N., 2001. Sensitivities of seismic velocities to temperature, pressure and composition in the lower mantle, *Phys. Earth planet. Inter.,* **124**(3–4), 255–267.

Tsuchiya, T., 2003. First-principles prediction of the P-V-T equation of state of gold and the 660-km discontinuity in Earth's mantle, *J. geophys. Res.,* **108,** 2462, doi:10.1029/2003JB002446.

Tsuchiya, T. & Tsuchiya, J., 2006. Effect of impurity on the elasticity of perovskite and postperovskite: velocity contrast across the postperovskite transition in $(Mg,Fe,Al)(Si,Al)O_3$, *Geophys. Res. Lett.,* **33,** L12S04, doi:10.1029/2006GL025706.

Tsuchiya, T. & Wang, X., 2013. Ab initio investigation on the high-temperature thermodynamic properties of Fe^{3+}-bearing $MgSiO_3$ perovskite, *J. geophys. Res.,* **118**(1), 83–91.

Umemoto, K., Hsu, H. & Wentzcovitch, R.M., 2010. Effect of site degeneracies on the spin crossovers in (Mg, Fe)SiO_3 perovskite, *Phys. Earth planet. Inter.,* **180**(3–4), 209–214.

Walter, M.J., Kubo, A., Yoshino, T., Brodholt, J., Koga, K.T. & Ohishi, Y., 2004. Phase relations and equation-of-state of aluminous Mg-silicate perovskite and implications for Earth's lower mantle, *Earth planet. Sci. Lett.,* **222,** 501–516.

Wentzcovitch, R.M., Karki, B.B., Cococcioni, M. & de Gironcoli, S., 2004. Thermoelastic properties of $MgSiO_3$-perovskite: insights on the nature of the Earth's lower mantle, *Phys. Rev. Lett.,* **92**(1), doi:10.1103/PhysRevLett.92.018501.

Wicks, J.K., Jackson, J.M. & Sturhahn, W., 2010. Very low sound velocities in iron-rich (Mg,Fe)O: implications for the core-mantle boundary region, *Geophys. Res. Lett.,* **37,** L15304, doi:10.1029/2010GL043689.

Williams, Q. & Garnero, E.J., 1996. Seismic evidence for partial melt at the base of Earth's mantle, *Science,* **273**(5281), 1528–1530.

Wookey, J., Stackhouse, S., Kendall, J.M., Brodholt, J. & Price, G.D., 2005. Efficacy of the post-perovskite phase as an explanation for lowermost-mantle seismic properties, *Nature,* **438**(7070), 1004–1007.

Yagi, T., Okabe, K., Nishiyama, N., Kubo, A. & Kikegawa, T., 2004. Complicated effects of aluminum on the compressibility of silicate perovskite, *Phys. Earth planet. Inter.,* **143–144,** 81–91.

Yamanaka, T., Mao, W.L., Mao, H.-K., Hemley, R.J. & Shen, G., 2010. New structure and spin state of iron-rich (Mg,Fe)SiO_3 post-perovskite, *J. Phys. Conf. Ser.,* **215,** doi:10.1088/1742-6596/215/1/012100.

Yu, Y.G., Hsu, H., Cococcioni, M. & Wentzcovitch, R.M., 2012. Spin states and hyperfine interactions of iron incorporated in $MgSiO_3$ post-perovskite, *Earth planet. Sci. Lett.,* **331–332,** 1–7.

Zhang, F. & Oganov, A.R., 2006. Valence state and spin transitions of iron in Earth's mantle silicates, *Earth planet. Sci. Lett.,* **249**(3–4), 436–443.

Zhang, L., Meng, Y. & Mao, W.L., 2012. Effect of pressure and composition on lattice parameters and unit-cell volume of (Fe,Mg)SiO_3 perovskite, *Earth planet. Sci. Lett.,* **317–318,** 120–125.